Available online at www.sciencedirect.com
ScienceDirect
Journal of Power Sources 173 (2007) 755–764
JOURNAL OF POWER SOURCES
www.elsevier.com/locate/jpowsour

The effect of receptor-polymer matrix compatibility on properties of PEO-based polymer electrolytes containing a supramolecular additive Part 1. Studies on phenomenon of compatibility

M. Pawłowska [a], G.Z. Żukowska [b], M. Kalita [b,*], A. Sołgała [b], P. Parzuchowski [a], M. Siekierski [b]

[a] *Department of Polymer Chemistry and Technology, Chemical Faculty, Warsaw University of Technology, Koszykowa 75, PL-00662 Warsaw, Poland*
[b] *Polymer Ionics Research Group, Chemical Faculty, Warsaw University of Technology, Noakowskiego 3, PL-00664 Warsaw, Poland*

Available online 26 May 2007

Abstract

This paper presents the results of studies of poly(ethylene oxide)-based solid polymer electrolyte with the addition of anion receptor. The main stress is put on the influence of the anion receptor-polymeric matrix compatibility on the morphology of the composite. The comparison of the properties of two supramolecular compounds (calix[4]arene derivatives) having identical groups active in anion coordination in the narrow rim but with wide rim modified by groups having structure non-compatible and compatible to poly(ethylene oxide), is analyzed. The research of the system is made by means of vibrational (both IR and Raman) spectroscopies to evaluate the anion receptor-polymer–salt interactions. Raman and EDS mapping are used to determine the local concentration of the additive and salt. DSC and XRD determine the membrane crystallinity. Imaging techniques (both SEM and polarized light micrographs) allow to observe the morphology of membrane surface. The presented results show that additive distribution depends on the type of the receptor used and the phase of the polymer matrix (amorphous or crystalline).

Keywords: Anion coordination; Vibrational spectroscopy; Structure–property relationships; Polymeric electrolyte

1. Introduction

Poly(ethylene oxide)-based (PEO-based), solid polymer electrolytes (SPEs) are well established products used in several applications, due to their low impact on environment, relatively low cost and no risk of electrolyte leakage (good usage safety) as well as good stability [1–3]. Unfortunately, two main disadvantages limit their wider commercial usage: low ionic conductivity – below 10^{-3} S cm^{-1} at 60 °C and below 10^{-5} S cm^{-1} at ambient temperature for PEO-LiX-ceramic filler composites- [4] in combination with low lithium transference number t_{Li^+} – in most cases, below 0.4 [5–8]. These properties are of different origin. Low σ is a result of the poor salt dissociation. Typically, in SPE for applicable salt concentrations we observe mostly ionic aggregates instead of "free" cations and anions [9–11]. Low t_{Li^+} results from stronger interaction of Li^+ cations with the polymer matrix in comparison with the one observed for the corresponding anions which, in consequence, leads to the higher mobility of the anions in comparison with Li^+ cations [12–14].

Therefore, the improvement of the SPE electrical properties should focus on both anion immobilization to improve t_{Li^+} and the enhancement of the σ value. Unfortunately, the σ improvement in majority of the known systems causes lowering of t_{Li^+} and *vice versa* (e.g. [15,16]). In consequence, the development of the metallic lithium anode battery with an SPE membrane which would have low enough inner resistance and good stability of the electrode–electrolyte interface is still impossible.

One of the methods of anion immobilization and, thus, of t_{Li^+} improvement is the addition of anion coordinating compounds. One of the most interesting approaches is that a neutral macrocyclic molecule (supramolecular additive) being capable of forming a complex with the used anion via number of the interacting centers is used as an anion-coordinating compound. The increase of the t_{Li^+} value after supramolecular polymer

* Corresponding author. Tel.: +48 665 244 288; fax: +48 22 628 27 41.
E-mail address: michalka@soliton.ch.pw.edu.pl (M. Kalita).

0378-7753/$ – see front matter © 2007 Elsevier B.V. All rights reserved.
doi:10.1016/j.jpowsour.2007.05.087

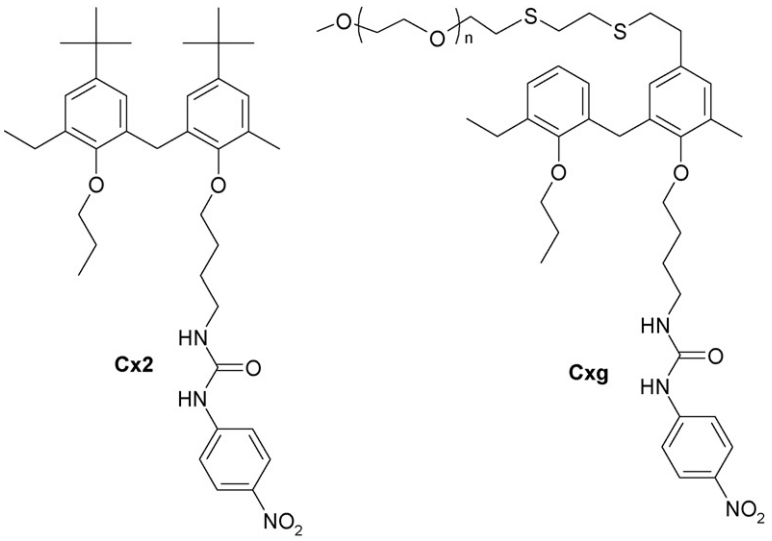

Fig. 1. **Cx2** and **Cxg** formulas.

electrolyte modification was confirmed experimentally by group of Wieczorek and co-workers [17] (for calix[4]arene derivatives) and, theoretically, by *ab initio* calculations (for aza-cryptands) [18] by Johansson et al. We have previously examined various calix[4]arene derivatives with urea groups in the lower rim [19]. The application of this class of receptors as SPE additives improved t_{Li^+}, however, the conductivity of the membrane was lowered by at least one order of magnitude. This phenomenon could be attributed first of all to the decrease of the charge carriers concentration due to anion trapping and, additionally, to the high affinity of the carbonyl oxygen atom from the urea group to the Li^+ cation. Therefore, the application of calix[*n*]pyrrole derivatives which do not contain any atoms with possible strong interaction with cations (e.g. ether or carbonyl oxygen atoms) [20] was studied. An improvement of the t_{Li^+} was achieved but the limited solubility of the receptor in the polymer matrix was observed leading to the formation of the calyx[6]pyrrole aggregates [21]. Modeling studies of this type of additives (*meso*-octamethylcalix[4]pyrrole) performed by Johansson and Jacobsson [22] also confirmed the anion-receptor complex formation.

Taking into consideration the discrepancies in the electrochemical and spectroscopic properties of various (in terms of the molecular weight of the applied polymer matrix) calix-type compounds containing composites the issue of the interactions between polymeric solvent and receptor raised. To study this subject we have concentrated on 5,11,17,23-tetra-*p*-*tert*-butyl-25,27-bis(((*N*-*p*-nitrophenylureido)butyl) oxy)-26,28-dipropoxycalix[4]arene (**Cx2**) receptor [23] and compared the obtained results with those presented by Scheerder et al. [24] for a similar anion trap of different urea substituent. The estimated solvent molecule-receptor complex formation gave semi-quantitative information about the competitive PEO-receptor and anion-receptor showing the possibility of the application of the calix[4]arene derivatives in samples based on solid high molecular weight polymer. Following this route and taking into consideration the limited solubility of the supramolecular additive in the polymer host, we decided to study the differences in the properties of the composite electrolytes containing two anion receptors **Cx2** and calix[4]arene derivative **Cxg** with identically modified narrow rim but with two polyoxyethylene chains instead of four *tert*-butyl in the wide rim (**Cxg**, Fig. 1). Both compounds contain two urea groups in their structure and should be similarly able to complex anions. The **Cxg** receptor should reveal a better compatibility with the polymer host due to the presence of identical structural units in its molecule. Thanks to this phenomenon, the additive particles agglomeration should be overcome due to their anchoring to the polymer chains. Addition of both anion receptors to the pristine PEO–salt system can also result in the change of the physical cross-linking density due to their impact on the observed ionic equilibriums, and crystallinity with the related crystal morphology of the polymer phase, due to above mentioned anion receptor-PEO interactions.

2. Experimental

2.1. Membrane sample preparation

All preparative operations were performed in an argon glove box with humidity level below 3 ppm.

ACN and CH_2Cl_2 (both POCH, for DNA synthesis, water content below 10 and 50 ppm, respectively) were used as received. Salts (both Aldrich, 99.995% $LiCF_3SO_3$, 99% LiI) and PEO (Aldrich, average $M_W = 5 \times 10^6$) were dried for over 72 h at temperature up to 100 °C under high vacuum ($<10^{-4}$ mmHg).

The synthesis of **Cx2** and **Cxg** was conducted as in Refs. [19,25], respectively. The preparation of the electrolyte samples was conducted as in Ref. [26]. The electrolyte was obtained by casting the mixture of the two separately prepared solutions: salt and PEO in CH_3CN and **Cx2** (or **Cxg**) in CH_2Cl_2 and dried using the procedure described in the ref. above. All samples were prepared maintaining ether oxygen atoms to lithium cations molar ratios equal to 20:1. For the **Cxg**-containing ones

the oligo(ethylene oxide) chains present in the receptor were counted into the total number of the ether oxygen atoms present in the sample. The salt to receptor ratio was always equal to 3:1.

2.2. SEM images

SEM images were taken using a FEI Quanta 200 microscope with an EDAX EDS analyzer. To preserve the properties and crystalline structure of the tested membranes all operations of the sample preparation were performed in a dry-box and the beam current was minimized to avoid the thermal effect of the beam (sample melting). The low vacuum mode was used for both image gathering and the EDS analysis.

2.3. FT-IR spectroscopy

Infrared absorption spectra were recorded on a computer interfaced Perkin-Elmer 2000 FT-IR system with a wavenumber resolution of 1 cm^{-1}. The spectra were performed for samples dispersed in KBr pellets or as films using HATR accessory with ZnSe crystal. For KBr pellets, spectra were recorded at 25 °C, and for films at 50 °C. FT-IR spectra were analyzed using a Galactic Grams Research software package using a Gaussian–Lorentzian function [27,28].

2.4. Raman spectroscopy

Raman spectra were collected using a Nicolet Almega Raman dispersive spectrometer, equipped with a confocal Raman microscope, a 1800 lines mm^{-1} holographic grating and a CCD camera. A diode laser operating at 780 nm was used as the excitation source and spectral resolution was about 2 cm^{-1} for high resolution spectra. In order to avoid contact with air during the measurements, the samples were kept in sealed glass containers. All spectra were recorded at 25 °C. For mapping experiments, spectra were collected using 360 lines mm^{-1} holographic grating and resolution was about 10 cm^{-1}. The exposure time was typically 15–20 s for mapping experiments and 60–120 s for high resolution spectra.

2.5. XRD studies

Laboratory X-ray powder diffraction patterns were recorded on a Seifert HZG-4 automated diffractometer using Cu Kα radiation (λ = 1.5418 Å). The data were collected in the Brag–Brentano ($\theta/2\theta$) horizontal geometry (flat reflection mode) between 5° and 60° (2θ) in 0.04° steps, at 2 or 3 s $step^{-1}$. The optics of the HZG-4 diffractometer was a system of primary Soller slits between the X-ray tube and the fixed aperture slit of 2.0 mm. One scattered-radiation slit of 2 mm was placed after the sample, followed by the detector slit of 0.35 mm. All samples were placed on the glass support and kept sealed during the experiment with a self-adhesive tape. The collected data were baseline corrected. The signal intensity was normalized taking into consideration different sample thickness and sweeping velocity.

2.6. DSC

DSC data were collected using a Perkin-Elmer Pyris 1 DSC at the heating rate of 20 °C min^{-1} in −120 to 250 °C temperature range. The degree of the crystallinity measured by means of DSC was calculated according to the equation $X_c = Q_m Q_{PEO}^{-1}$, where Q_m is a latent melting heat for the polyether used and $Q_{m,PEO}$ is latent melting heat found for the crystalline P(EO) phase. According to the literature, $Q_{mPEO} = 213.7$ J g^{-1} [26,29].

3. Results

3.1. SEM images

The SEM images of the PEO-LiTf-**Cx2** and **Cxg** composites are depicted in Figs. 2a and b and 3a, respectively. One can observe that the studied systems reveal different morphology: PEO-LiTf-**Cx2** crystallizes forming "sponge-like" structures, PEO-LiTf-**Cxg** forms large spherulites. In contrast, in the case of LiI-containing systems (Figs. 2c and d and 3b) no specific structures separation can be observed with the spherulitic structure still maintained. It can be also observed that volume of the interspherulitic amorphous phase for **Cx2** containing sample is significantly larger than for **Cxg** containing one. Fig. 4 shows the comparison of the SEM image of the sample with EDS intensity mapping for two elements: carbon characteristic mainly for the receptor and, partially, for the polymer phase and sulfur which is present in the salt. Image 4a shows a well defined boundary between the two spherulites. The carbon line intensity follows exactly the SEM image also revealing the phase boundary while the sulfur concentration profile is much more uniform. This observation proves that salt is located evenly in both spherulites (being heterophase systems themselves) and in the inter-spherulitic amorphous phase, while receptor concentration is significantly higher in the interspherulitic areas than in spherulites.

3.2. FT-IR spectroscopy

The formation of complex between calixarene receptors and anions was studied using FT-IR spectroscopy. The hydrogen bond formation between the amide group of the receptor and the anion (or polymer) results in the change of several amide characteristic bands. The most pronounced changes are observed for bands of the C=O stretching vibrations. Fig. 5 shows a comparison of the carbonyl stretching region in FT-IR spectra of PEO-**Cx2**, PEO-**Cx2**-LiI and PEO-**Cx2**-$LiCF_3SO_3$ samples. In the spectrum of the PEO-**Cx2** sample the band of C=O stretching vibration is split into a doublet with two distinct maxima, at 1710 and 1676 cm^{-1}. The peak at 1710 cm^{-1} corresponds to the free carbonyl group and that at 1676 cm^{-1} can be a superposition of peaks attributed to weakly and strongly associated carbonyl groups, with maxima respectively at ∼1680 and 1640 cm^{-1}. In spectra of samples containing lithium salt the maximum of the peak is slightly shifted towards lower wavenumbers (1707 and 1705 cm^{-1} for $LiCF_3SO_3$ and LiI, respectively) and bands of

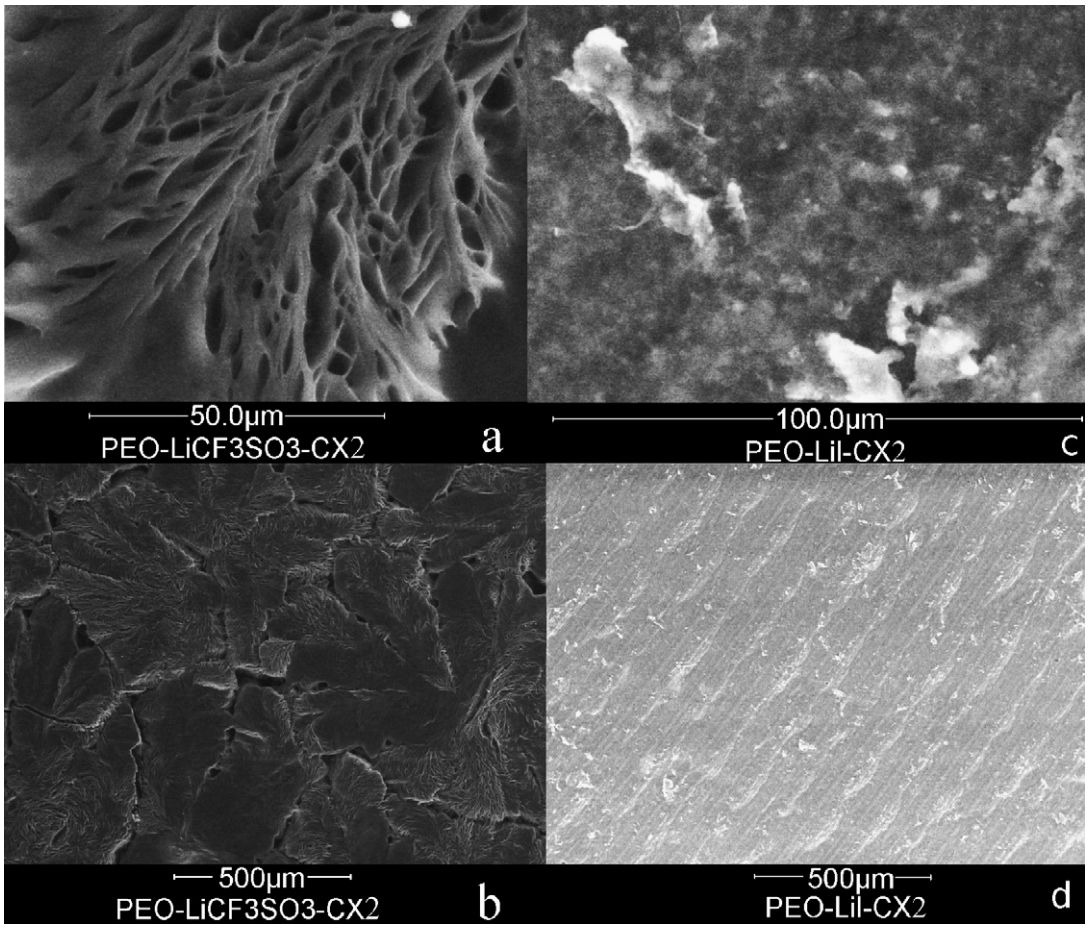

Fig. 2. SEM images—**Cx2**-containing systems.

the free and associated carbonyl groups are highly overlapped. It should be stressed here that the band is much broader for the PEO-**Cx2**-$LiCF_3SO_3$ than for PEO-**Cx2**-LiI sample. Additionally, the low frequency shoulder which appears at $\sim$1675 cm^{-1} for the triflate doped electrolyte shifts to $\sim$1690 cm^{-1} for the iodide containing one. The described effect may indicate that salt addition results in breaking stronger hydrogen bonds linking **Cx2** molecules and formation of weaker ones between anions and **Cx2**. The broadening of the band in spectra of lithium salt-doped membranes may also indicate some interactions between the lithium cation and the carbonyl group of the receptor.

3.3. Raman spectroscopy

The obtained membranes doped with **Cx2** were all heterogeneous and highly crystalline. Optical polarized light microscope images (see Fig. 6) show that the diameter of spherulites is between 50 and 200 µm and Fig. 7 presents distribution of calixarene in PEO-**Cx2** matrix. It can be seen that the amor-

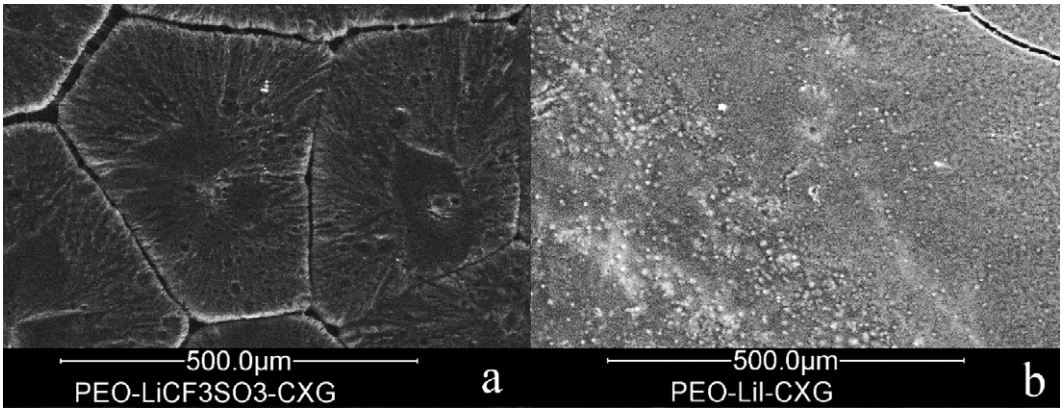

Fig. 3. SEM images—**Cxg**-containing systems.

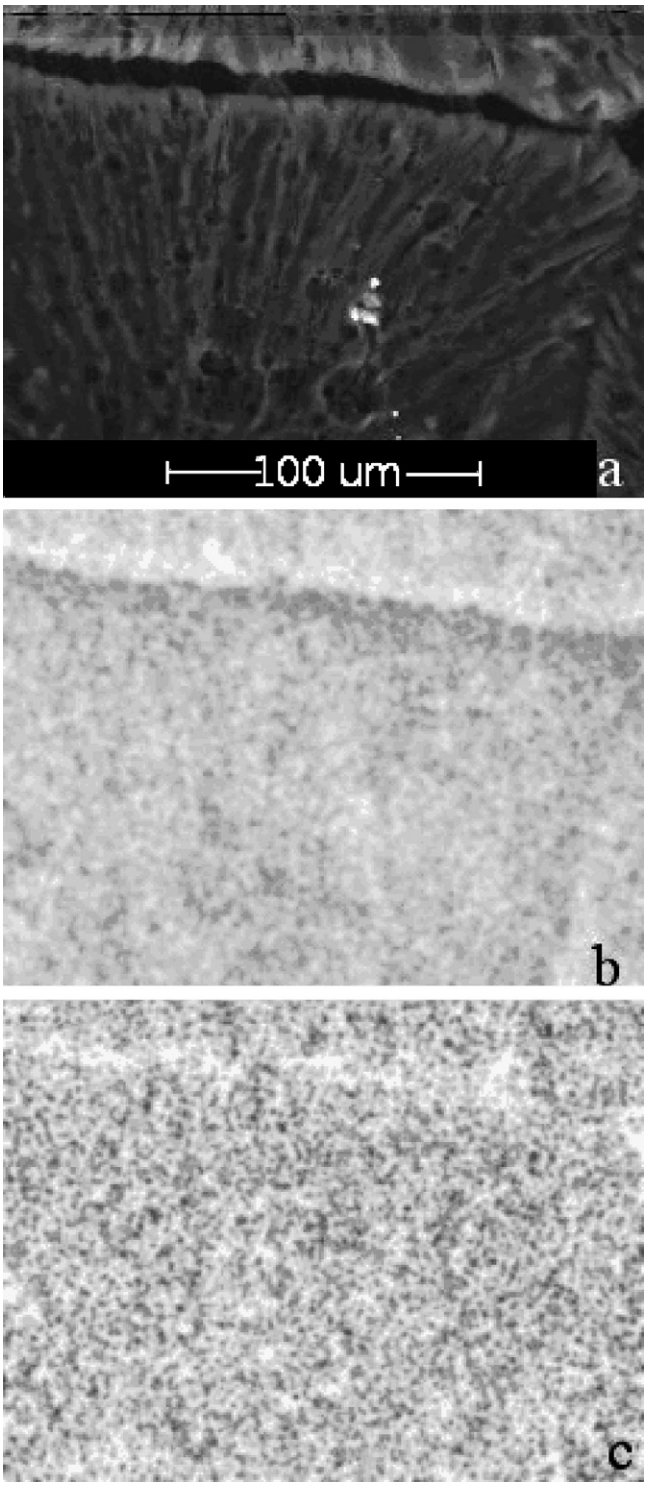

Fig. 4. EDS images of the PEO-LiTf-**Cxg** sample. (a) SEM image of the area; (b) carbon K line intensity mapping; (c) sulfur K line intensity mapping.

phous domains of membrane are richer in calixarene than the crystalline ones.

In order to study complexation of salt both by calixarene and the polymer matrix, we analyzed Raman spectra recorded in crystalline and amorphous parts of membranes. The band of the $\delta_{s\,CF_3}$ vibration of triflate anion is particularly useful to study

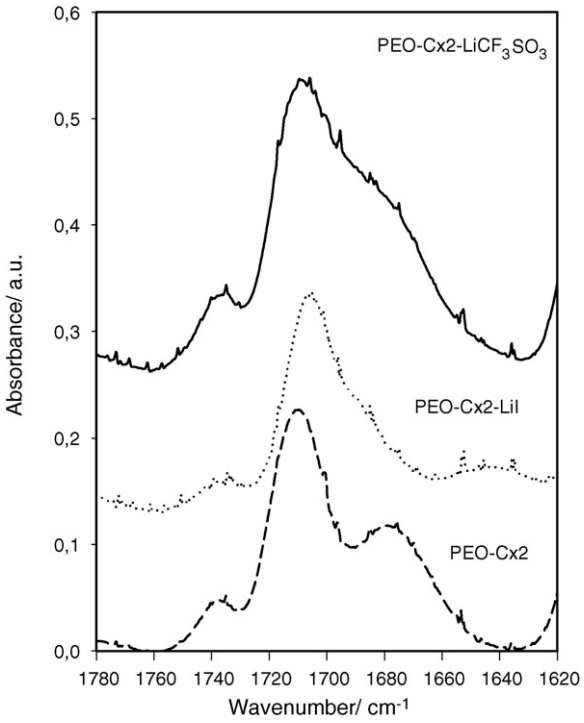

Fig. 5. FT-IR spectra of PEO membranes doped with **Cx2**.

complex formation. Fig. 8a and b shows deconvolution of the $\delta_{s\,CF_3}$ band for the spectrum taken in the crystalline and amorphous parts of the PEO-$LiCF_3SO_3$ membrane. In the crystalline phase the maximum of this band is centered at 755 cm^{-1}, while in the amorphous domains it is shifted to 759 cm^{-1} and has a much stronger intensity. According to the literature, various ionic species should give bands at ~753, ~758 and ~763 cm^{-1}, being ascribed to free anions, ionic pairs and triplets, respectively. In the spectrum taken in crystalline domains, the peak can be resolved using two contributions, with maxima at 757 and 753 cm^{-1}. The share of former is between 50 and 70%. For the amorphous domain, the band was split into contributes peak-

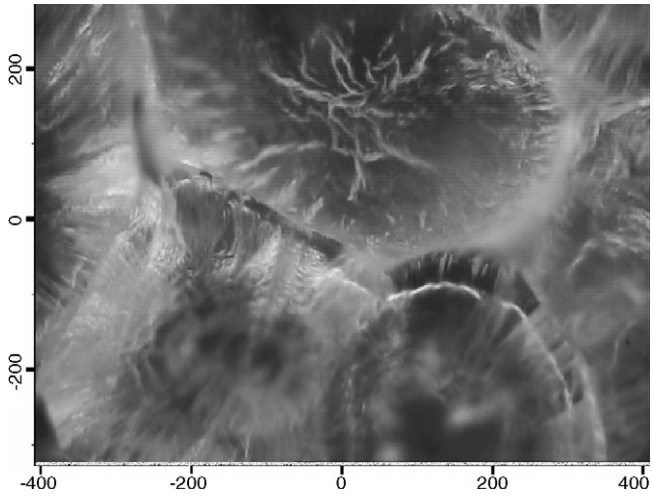

Fig. 6. Polarized light optical microphotograph of the PEO-**Cx2** film (distances in μm).

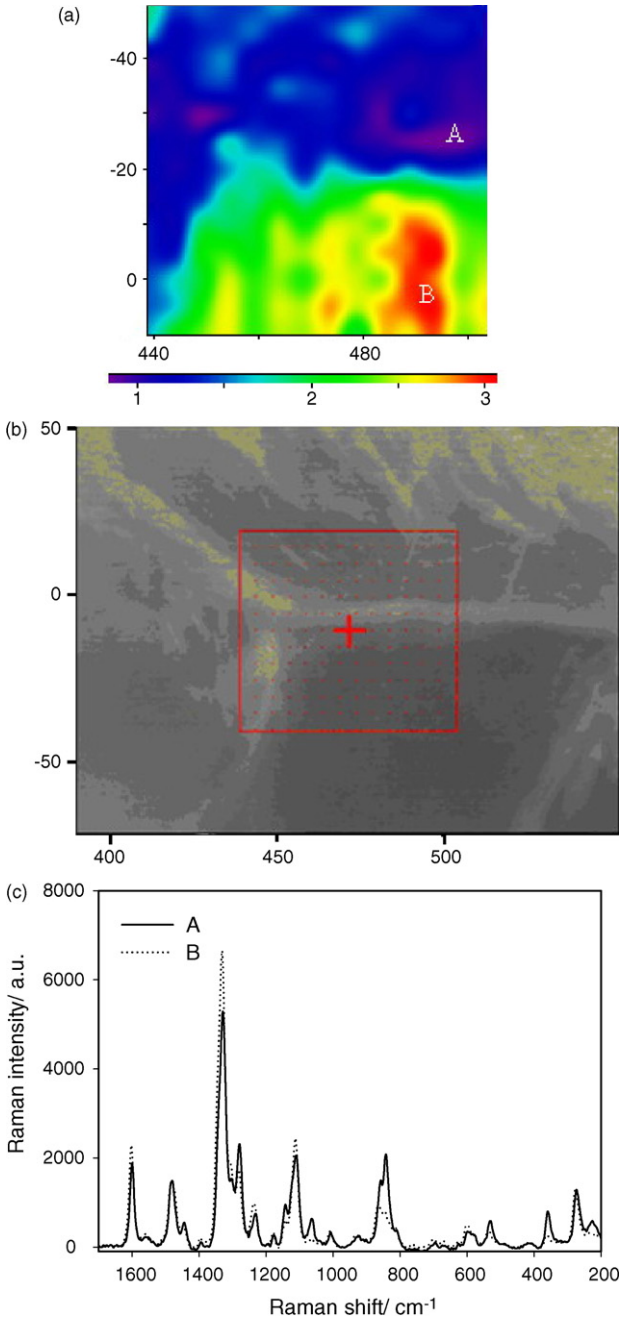

Fig. 7. (a) Map of intensity ratio of characteristic peaks of **Cx2** (ring stretching, 1600 cm^{-1}) and of crystalline phase of PEO (CH_2 rocking, 842 cm^{-1}) for PEO-**Cx2**. (b) Photo of the mapped membrane from CCD camera. (c) Raman spectra recorded in A and B areas. Scale in both maps in micrometers (μm).

ing at 759 and 756 cm^{-1}. The share of the latter is 58%, and of the former 42%.

Different results were obtained using band of the $\nu_{s\,SO_3}$ vibration. In this case, for the amorphous domain, the deconvolution gives three bands with maxima at 1054 cm^{-1} (triplets, 14%), 1043 cm^{-1} (ionic pairs, 62%) and 1031 cm^{-1} (free ions, 24%). For the crystalline phase, we were able to resolve this band into two contributes with maxima at 1040 cm^{-1} (ionic pairs, 32%) and 1030 cm^{-1} (free ions, 68%).

We obtain similar results for the PEO-**Cx2**-$LiCF_3SO_3$ membranes. Deconvolution of the $\delta_{s\,CF_3}$ peak gave 62% of ionic pairs and 38% of free anions for the crystalline phase, and 68% of ionic pairs and 32% of free anions for the amorphous phase. For the band of $\nu_{s\,SO_3}$ vibration mode in the amorphous phase we get the same share of ionic pairs (68%) and free anions (32%) as for membrane without **Cx2**. In the crystalline phase, the content of free ions was lower than in PEO-$LiCF_3SO_3$ sample and equal to 60% while share of ion pairs was almost the same (34%). However, we must stress that the studied membranes were heterogeneous and that the estimated values of the ionic species are dependent on the crystallinity degree. Comparing the spectra normalized against the intensity of $\delta_{s\,CF_3}$ peak of $LiCF_3SO_3$ we also observed that the intensity ratio of ring stretching vibration of **Cx2** (maximum at 1598 cm^{-1}) and of $\delta_{s\,CF_3}$ is much higher in the amorphous phase (see Fig. 3).

These observations are confirmed by Raman mapping. Fig. 9 presents Raman map for PEO-**Cx2**-$LiCF_3SO_3$ obtained by comparing intensities of peaks of ν_{ring} (**Cx2**) and $\delta_{s\,CF_3}$ (salt). The **Cx2**/salt concentration ratio is higher in the amorphous domains of the sample, and lower in the crystalline ones. These results correspond to those obtained for the PEO-**Cx2** membrane (without salt), where, as seen in the Raman map shown in Fig. 7, **Cx2** was aggregated in amorphous domains.

A similar effect, i.e. relatively higher content of free ions in the crystalline phase and higher content of calixarene in the amorphous phase was found for membrane containing **Cxg**.

Both membranes without the macrocyclic compound PEO-$LiCF_3SO_3$ and PEO-LiI were crystalline but the crystallinity was higher for the iodide doped sample. Fig. 10 shows comparison of Raman spectra for PEO-$LiCF_3SO_3$, PEO-LiI, PEO-$LiCF_3SO_3$-**Cx2** and PEO-LiI-**Cx2**, recorded in the crystalline areas of samples. It can be seen that the intensity of peaks at 1272 and 835 cm^{-1}, which are characteristic for the crystalline phase, is the strongest for the PEO-LiI sample. The addition of receptors resulted in a decrease of crystallinity for all systems studied but this effect was more pronounced for iodide-doped samples. We found that crystallinity also decreased for the sample without the lithium salt which is consistent with FT-IR data, indicating formation of hydrogen bonds between ether oxygen of PEO and urea moieties of the receptor. The application of the substituted calixarene as anion receptor improves the homogeneity of the membrane. Fig. 11 shows a comparison of the Raman spectra extracted from the Raman map of the PEO-LiI-**Cxg** membrane. Only slight differences for spectra recorded in various areas of the sample can be found.

3.4. XRD studies

When comparing the plots obtained for all samples containing **Cx2** (Fig. 12) with the diffractogram of the pure supramolecular compound (Fig. 13) one can easily observe that even in the case of the salt free membrane the complete amorphisation of the calix[4]arene derivative is observed. This observation proves that even high molecular weight polyether somehow interacts with the receptor. Additionally, a comparison of the plots obtained for the pristine samples (Fig. 14) with

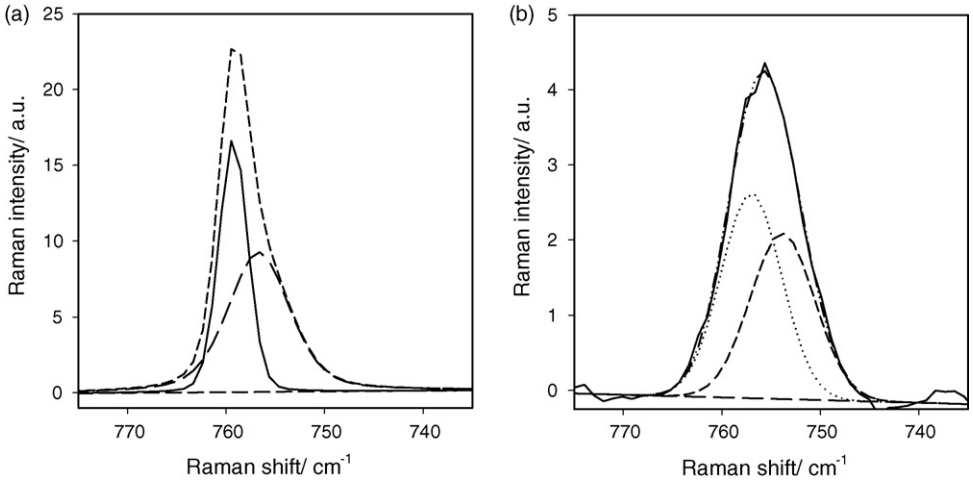

Fig. 8. Deconvolution of the $\delta_{s\,CF_3}$ band in Raman spectrum of amorphous (a) and crystalline (b) domains of PEO-$LiCF_3SO_3$ membrane.

the ones containing the additive shows clearly that the modified membranes exhibit a stronger amorphous bump around the PEO reflections. This phenomenon can be also attributed to the polymer-receptor interactions. The distortion effect is stronger for the **Cx2** receptor what shows that the negative interactions of the **Cxg** derivative with the crystalline PEO phase is weaker. Finally, the crystallinity data are gathered in Table 1. The obtained value was calculated by the integration of the area characteristic for the peak located near $2\theta = 19^\circ$ and is characteristic for the crystalline phase of pure polymer. A $(PEO)_{10}$LiI sample was used as a reference with crystallinity degree equal to 70%. The results show that the LiTf containing samples are generally less crystalline than the ones doped with LiI. Additionally, both compounds lead to the amorphisation of the triflate containing composites while the crystallinity of iodide complexes remains almost unchanged. In the first case the **Cx2** compound reveals a stronger amorphisation activity in comparison to **Cxg**. The intensity of the second peak typical for the PEO crystalline phase was also analyzed. The study shows that for some samples the intensity of the peak is much larger than the one which should be predicted on the basis of the crystalline phase content. Additionally, the peak maximum is slightly shifted and/or the peak can be split. This phenomenon is related to the formation of the crystalline polymer salt complex characterized with a much higher specific reflexivity. The intensity of the signal is, thus, a combination of two unequal contributions and cannot be easily interpreted quantitatively.

3.5. DSC

A typical DSC trace for the PEO-lithium salt system presents two signals: the first one (baseline shift) characteristic for the second order transition is observed between −40 and −10 °C and can be assigned to the glass transition while the second one (endothermic peak) is located between 60 and 75 °C and can be attributed to the melting of the PEO crystalline phase [30–32]. The DSC trace for PEO-LiTf-**Cx2** systems which is typical for all samples containing anion receptor as an additive is depicted in Fig. 15. In contrast to previous results of our group [18,19], no heat effect related to the crystalline PEO-salt complex melting was observed. Table 2 gathers the temperature of the crystalline phase melting, specific enthalpy of melting together with the calculated crystallinity degree. The normalized values are obtained on the basis of pure PEO mass fraction in the studied composition. The comparison of the values obtained for PEO and PEO-**Cx2** samples shows that the addition of this supramolecular additive does not prevent the crystallization of the polymer. In the case of the salt containing samples the **Cx2** presence even promotes the matrix crystallization. Remarkably, an important observation can be made for the **Cxg** composites. Here the normalized crystallinity values are extremely and unreasonably high. This effect clearly shows that the excess heat effect observed must be related with the co-crystallization of the oligooxyethylene chains of the receptor with the PEO matrix. Therefore, a previously mentioned link between these

Table 1
XRD crystallinity data gathered for the studied electrolytes

Sample	Thickness (μm)	$2\theta = 19^\circ$ (a.u.)	$2\theta = 23^\circ$ (a.u.)	$2\theta = 19^\circ$ corrected	$2\theta = 23^\circ$ corrected	X_c
PEO-**Cx2**	135	3759	12,552	27,840	92,750	0.79
PEO-LiI	117	2889	4,274	24,690	36,530	0.70
PEO-LiTf	131	1750	9,728	13,318	74,030	0.38
PEO-LiI-**Cx2**	73	1703	4,794	23,580	66,390	0.67
PEO-LiTf-**Cx2**	149	623	2,965	4,158	19,790	0.12
PEO-LiI-**Cxg**	63	1486	3,506	23,587	55,650	0.67
PEO-LiTf-**Cxg**	55	630	3,148	11,454	57,236	0.33

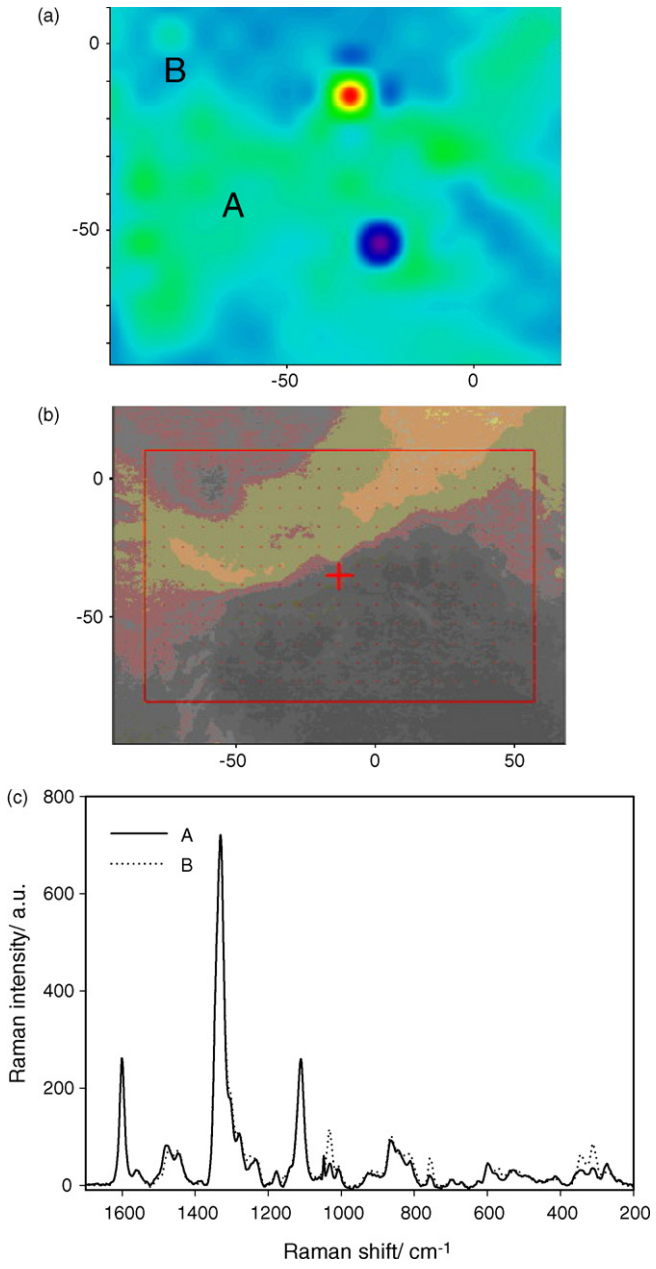

Fig. 9. (a) Map of intensity ratio of characteristic peaks of **Cx2** (ring stretching, 1600 cm^{-1}) and of $LiCF_3SO_3$ ($\delta_{s\,CF_3}$, 758 cm^{-1}) for PEO-**Cx2**- $LiCF_3SO_3$. (b) Photo of the mapped membrane from CCD camera. (c) Raman spectra recorded in A and B areas. Scale in both maps in micrometers (μm).

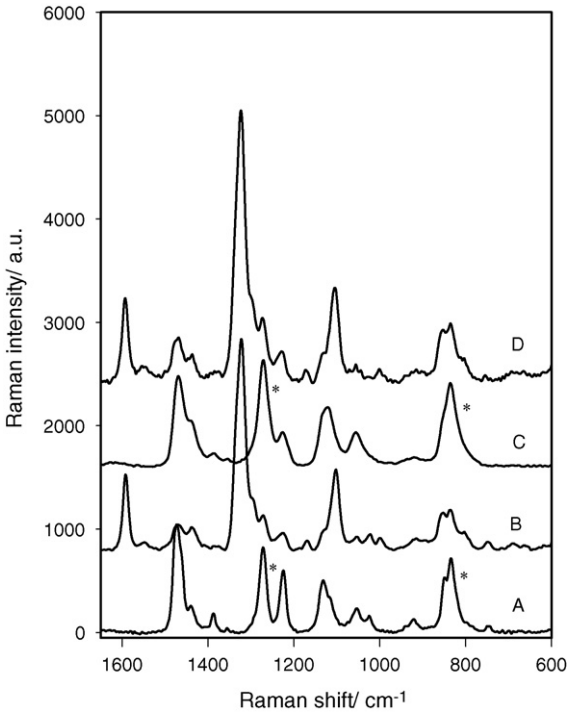

Fig. 10. Raman spectra of (A) PEO-$LiCF_3SO_3$; (B) PEO-$LiCF_3SO_3$-**Cx2**; (C) PEO-LiI; (D) PEO-LiI-**Cx2**. Bands characteristic for crystalline phase are indicated by asterisks.

two phases is observed confirming the better polymer-anion trap compatibility. The co-crystallization effect is stronger for LiTf containing samples.

4. Discussion

A comparison of the DSC and XRD crystallinity data shows that the observed discrepancy is stronger for LiTf containing samples in comparison with the LiI ones. XRD diffraction patterns shows the formation of the crystalline salt–PEO complex which cannot be observed in the DSC traces. The observed differences in the crystallinity degree prove that triflate salt promotes the formation of highly distorted crystalline phase (not observed in XRD and observed in DSC). The observed structure difference is not observed in SEM images where, in both cases (of course only qualitatively) a crystalline spherulitic structure can be observed. For both salts the addition of the **Cx2** receptor increases the DSC crystallinity and decreases the XRD one.

Table 2
Melting points, enthalpies of melting and DSC-based calculated crystallinites

Sample	T_m (°C)	H_m (J g^{-1})	X_c (%)	X_c^N (%)
PEO	80.1	183	85	85
PEO-**Cx2**	74.2	121	57	83
PEO-LiI	75.5	114	52	61
PEO-LiTf	72.2	110	51	61
PEO-LiI-**Cx2**	75.1	98	46	74
PEO-LiTf-**Cx2**	78.8	99	47	76
PEO-LiI-**Cxg**	63.5	73	34	84
PEO-LiTf-**Cxg**	75.5	83	39	98

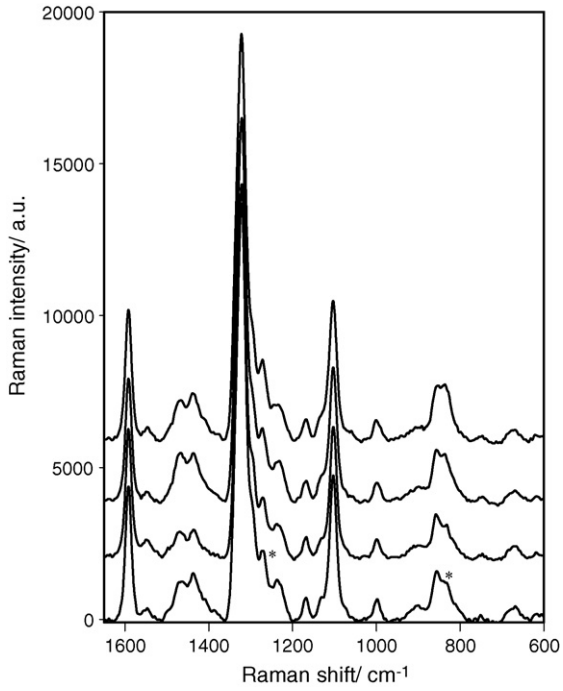

Fig. 11. Raman spectra recorded in different areas PEO-LiI-**Cxg** membrane. Bands characteristic for crystalline phase are indicated by asterisks.

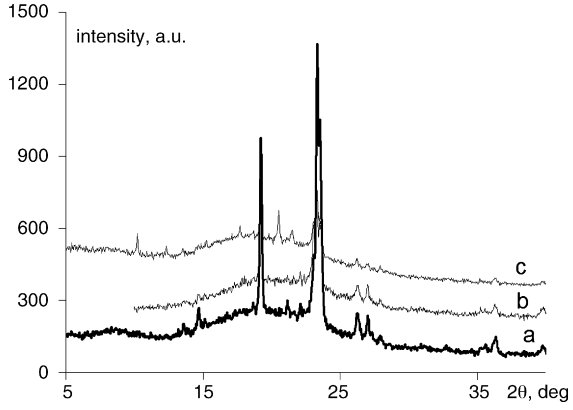

Fig. 12. Diffractograms of the samples containing **Cx2**: (a) no salt; (b) LiI; (c) LiTf.

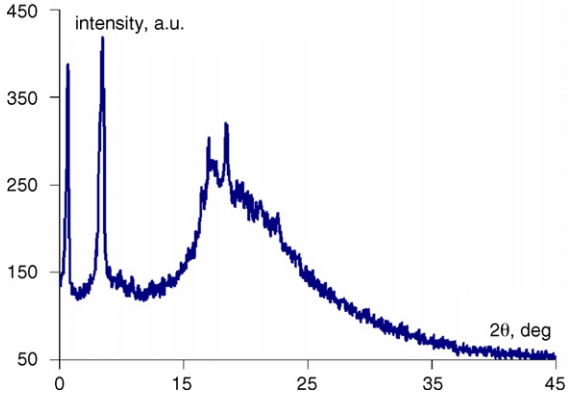

Fig. 13. Diffractogram of **Cx2** (powdered compound).

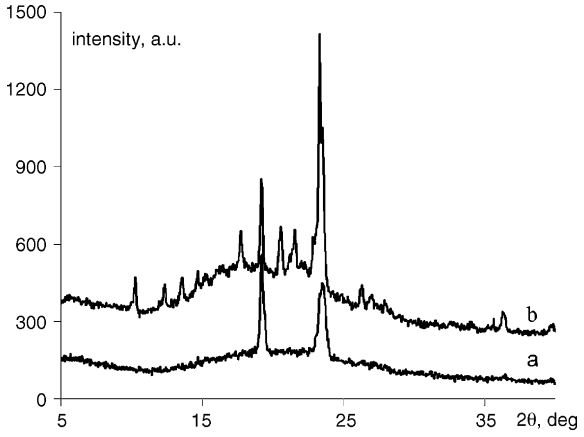

Fig. 14. Diffractograms of the pristine samples. (a) $(PEO)_{20}$LiI; (b) $(PEO)_{20}$LiTf.

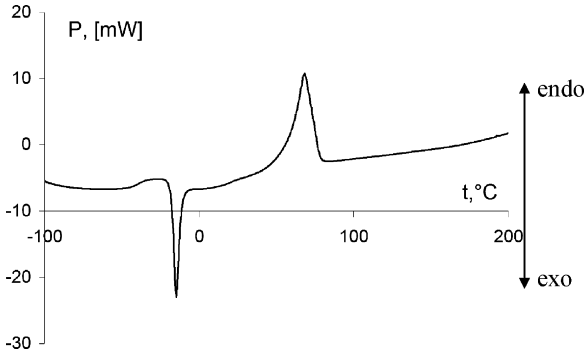

Fig. 15. DSC trace for PEO-LiTf-**Cx2** system.

This phenomenon is less pronounced for LiI samples. This fact shows that **Cx2** aggregates promotes crystallization (increases the total content of the crystalline phase observed in DSC) simultaneously deteriorating the quality of the crystalline phase by its defects (the lower fraction of the well defined crystallites observed in XRD and a stronger XRD amorphous bump). This observation is confirmed by the local Raman crystallinity probe showing that in the absence of the active filler the crystalline phase is of better quality in terms of the defects concentration. Raman spectroscopy gives the information on the local quality of the crystalline phase within the spherulite, thus, the obtained observations are of different nature than for both DSC and XRD where the global average phase composition is observed. For the pristine systems there is only a slight increase of the crystallinity for the LiI containing sample in comparison with LiTf containing one. This observation can be located between the XRD data revealing a strong discrepancy and identical DSC crystallinity values. For **Cx2** containing composites Raman spectroscopy does not reveal the salt type phase composition dependence being in accordance with the DSC results and in contrast with the XRD data. The Raman observations of the **Cxg** compound reveal a local microstructure of the composite similar to **Cx2** ones for both of the salts used. This observation is in contrast with the global values in which a co-crystallization of the **Cxg** is observed in DSC and a much lower quantity of the well defined crystallites is present in samples containing LiTf for both of the

receptors studied. In general, the tendencies observed in Raman data are more similar to the ones observed in DSC not in XRD.

5. Conclusions

The presented results show clearly that a better compatibility between the supramolecular receptor and the PEO polymer matrix can be achieved by the receptor molecule modification through introducing of two polyoxyethylene chains instead of four *tert*-butyl groups in the wide rim. The better compatibility of the **Cxg** receptor with the polymer host can be attributed to the presence of identical structural units in its molecule leading, in consequence, to the co-crystallization with the polymer phase. In this way the agglomeration of the additive particles is overcome by the anchoring to the polymer chains. Thus, the electrochemical stability of the newly introduced receptor should be analyzed together with the studies of the conducting properties of the obtained membranes.

Acknowledgements

This work was supported in part by the Polish Ministry of Science and Higher Education (3T08E01528) and in part by the Air Force Office of Scientific Research, Air Force Command, USAF, under grant no. FA8655-05-1-3014. Mr. Andrzej Łukaszewicz is kindly acknowledged for the proofreading of the manuscript. Prof. Władysław Wieczorek, Prof. Gabriel Rokicki and Dr. Michał Chmielewski are acknowledged for helpful comments and fruitful discussions. Special thanks are given to Henryk Wyciślik for his valuable comments on the XDR measurements.

References

[1] F.M. Gray, Solid Polymer Electrolytes. Fundamentals and Technological Applications, VCH Publishers, Weinheim, 1991.
[2] P.D. Bruce, Solid State Electrochemistry, Cambridge University Press, 1995.
[3] B. Scrosati, G. Stienen (Eds.), Applications of Electroactive Polymers, Kluwer Academic Publishers, 1993.
[4] F. Croce, G.B. Appetecchi, L. Persi, B. Scrosati, Nature 394 (1998) 456.
[5] J.M. Tarascon, M. Armand, Nature 44 (2001) 359.
[6] M. Watanabe, A. Nishimoto, Solid State Ionics 79 (1995) 306.
[7] F. Alloin, D. Benrabah, J.-Y. Sanchez, J. Power Sources 68 (1997) 372.
[8] H. Cheradame, J.-F. Lenest, A. Gandini, M. Leveque, J. Power Sources 14 (1985) 27.
[9] W. Wieczorek, D. Raducha, A. Zalewska, J.R. Stevens, J. Phys. Chem. B 102 (1998) 8725.
[10] M. Marcinek, M. Ciosek, G. Żukowska, W. Wieczorek, K.R. Jeffrey, J.R. Stevens, Solid State Ionics 176 (2005) 367.
[11] M. Marcinek, G.Z. Żukowska, W. Wieczorek, Electrochim. Acta 50 (2005) 3934.
[12] E. Staunton, Y.G. Andreev, P.G. Bruce, J. Am. Chem. Soc. 127 (2005) 12176.
[13] Z. Stoeva, I. Martin-Litas, E. Staunton, Y.G. Andreev, P.G. Bruce, J. Am. Chem. Soc. 125 (2003) 4619.
[14] A.M. Christie, S.J. Lilley, E. Staunton, Y.G. Andreev, P.G. Bruce, Nature 433 (2005) 50.
[15] D. Benrabah, S. Sylla, F. Alloin, J.-Y. Sanchez, M. Armand, Electrochim. Acta 40 (1995) 2259.
[16] J.M.G. Cowie, G.H. Spence, Solid State Ionics 123 (1999) 233.
[17] A. Błażejczyk, W. Wieczorek, R. Kovarsky, D. Golodnitsky, E. Peled, L.G. Scanlon, G.B. Appetecchi, B. Scrosati, J. Electrochem. Soc. 151 (2004) A1762.
[18] P. Johansson, Electrochim. Acta 48 (2003) 2291.
[19] A. Błażejczyk, M. Szczupak, W. Wieczorek, P. Ćmoch, G.B. Appetecchi, B. Scrosati, R. Kovarsky, D. Golodnitsky, E. Peled, Chem. Mater. 17 (2005) 1535.
[20] M. Kalita, M. Bukat, M. Ciosek, M. Siekierski, S.H. Chung, T. Rodríguez, S.G. Greenbaum, R. Kovarsky, D. Golodnitsky, E. Peled, D. Zane, B. Scrosati, W. Wieczorek, Electrochim. Acta 50 (2005) 3942.
[21] A. Plewa, F. Chyliński, M. Kalita, M. Bukat, P. Parzuchowski, R. Borkowska, M. Siekierski, G.Z. Żukowska, W. Wieczorek, J. Power Sources 159 (2006) 431.
[22] P. Johansson, P. Jacobsson, Electrochim. Acta 50 (2005) 3782.
[23] A. Plewa, M. Kalita, G.Z. Żukowska, A. Sołgała, M. Siekierski, ECS Trans. 3/12 (2006) 59.
[24] J. Scheerder, M. Fochi, J.F.J. Engbersen, D.N. Reinhoudt, J. Org. Chem. 59 (1994) 7815.
[25] M. Kalita, A. Sołgała, M. Siekierski, M. Pawłowska, G. Rokicki, W. Wieczorek, J. Power Sources, this issue.
[26] J. Przyłuski, W. Wieczorek, J. Therm. Anal. 38 (1992) 2229.
[27] C.P. Rhodes, R. Krech, Solid State Ionics 136–137 (2000) 1131.
[28] J.M. Alie, H.G.M. Edwards, Vibrat. Spectrosc. 24 (2000) 185.
[29] X. Li, S.L. Hsu, J. Polym. Sci., Polym. Phys. Ed. 22 (1984) 1331.
[30] J.E. Weston, B.C.H. Steele, Solid State Ionics 2 (1981) 347.
[31] Y.W. Kim, W. Lee, B.K. Choi, Electrochim. Acta 45 (2000) 1473.
[32] A. Vallee, S. Besner, J. Prud'Homme, Electrochim. Acta 37 (1992) 1579.